
Article:
Li, H.Y. and Zhu, Z.Q. orcid.org/0000-0001-7175-3307 (2018) Analysis of flux-reversal permanent-magnet machines with different consequent-pole PM topologies. IEEE Transactions on Magnetics, 54 (11). 8105305. ISSN 0018-9464

https://doi.org/10.1109/TMAG.2018.2839708

Analysis of Flux Reversal Permanent Magnet Machines with Different Consequent-Pole PM Topologies

H .Y. Li, *Student Member, IEEE,* and Z. Q. Zhu, *Fellow, IEEE*

Department of Electronic and Electrical Engineering, University of Sheffield, Sheffield, S1 3JD, U. K.

This paper comprehensively studies the electromagnetic performance of flux reversal permanent magnet (FRPM) machines with different consequent-pole PM (CPM) topologies. Four CPM topologies are firstly introduced and classified by different numbers of PM pieces and PM locations on stator teeth. Then, the distribution and working harmonics of air-gap flux density of each CPM topology are analyzed and compared, and the CPM topology with the highest torque density is identified. The influence of critical design parameters on machine performance is also parametrically investigated. By comparing the torque performance of CPM topologies with their surface-mounted PM (SPM) counterparts, the advantages of CPM topologies, i.e. torque improvement and magnet volume reduction, are clearly revealed. Four FRPM prototypes are manufactured and tested to verify the analyses.

***Index Terms*—Consequent-pole, end effect, flux reversal, permanent magnet.**

I. Introduction

FLUX reversal permanent magnet (FRPM) machines have advantages of robust rotor structure, simple stator structure and easy heat management of PMs, making them promising in low-speed and high-torque applications [1-6]. However, for conventional FRPM machines with PMs mounted on the inner surface of stator teeth, the large equivalent air-gap length resulted from surface-mounted PM (SPM) topology limits the field modulation effect of rotor teeth, thus impairing the torque performance [7, 8]. In [9], one kind of consequent-pole PM (CPM) topology is proposed to replace the SPM topology, which is beneficial to improve the armature field and the resulted torque, as well as to reduce the PM volume, as shown in Fig. 1(a). For each stator tooth, one PM piece together with the adjacent ferromagnetic iron pole make the magnitude and direction of flux through the coil vary with the relative rotor position. Moreover, the magnetization directions of PMs are identical for all the stator teeth, but the PM locations are different for two adjacent stator teeth. Therefore, the CPM topology can be designated as N/Fe-Fe/N.

In this paper, three new types of CPM topologies are proposed, as shown in Fig. 1(b)-(d), which are designated as N/Fe-N/Fe, N/Fe/N/Fe-Fe/N/Fe/N, and N/Fe/N/Fe-N/Fe/N/Fe, respectively. Similar to N/Fe-Fe/N (Type1), each stator tooth of N/Fe-N/Fe (Type2) has one PM piece and one ferromagnetic iron pole. However, the PM locations of all the stator teeth are identical. Both N/Fe/N/Fe-Fe/N/Fe/N (Type3) and N/Fe/N/Fe-N/Fe/N/Fe (Type4) have two PM pieces and two ferromagnetic iron poles on each stator tooth, and the PM locations of two adjacent stator teeth are different for the former, while they are exactly the same for the latter. Considering the fact that different CPM topologies directly influence the PM fields in air-gap and associated winding connections, their working harmonics and torque performance are quite different. Therefore, the analysis and comparison of various CPM topologies will be the main focus of this paper as it is of great significance for the design of FRPM machines aiming at high torque density and less PM usage.

Manuscript received ** **, 2018; revised ** **, 2018; accepted ** **, 2018. Date of publication ** **, 2018; date of current version ** **, 2018.
Corresponding author: Z. Q. Zhu (e-mail: z.q.zhu @sheffield.ac.uk).

II. Working Principle of FRPM Machines With Different CPM Topologies

Different from the conventional PM machines, in which the torque is only produced by the interaction between the main PM field and the main armature field having the same pole-pair number and rotational speed, the torque production mechanism of FRPM machine is quite complex since both PM magnetomotive force (MMF) and armature MMF are subjected to rotor-teeth modulation, resulting in abundant field harmonic pairs in air-gap. Typically, the pole pair number of the main harmonic of the PM field is not equal to that of the armature field, and this phenomenon is so called magnetic gearing effect or air-gap field modulation [10-13]. It has been proven that the torque of a conventional FRPM machine with SPM topology is contributed by the interaction of several harmonic pairs [8]. Considering that PM MMF distribution is changed and additional modulation is introduced due to the CPM topology, the distribution and working harmonics of air-gap flux density of FRPM machines with CPM topologies become more complex and deserve further investigation.

A. Air-gap Flux Density

Aiming at maximum torque density, four 14-pole-rotor FRPM machines with different CPM topologies are globally

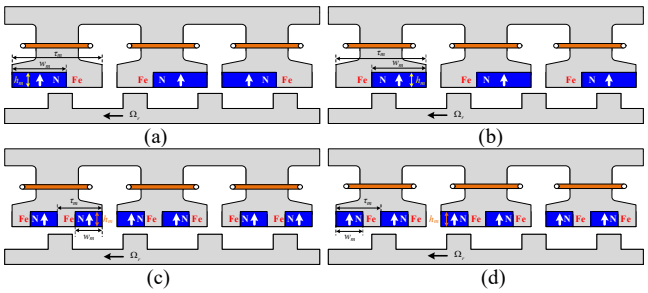

Fig. 1. FRPM machines with different CPM topologies. (a) Type1: N/Fe-Fe/N. (b) Type2: N/Fe-N/Fe. (c) Type3: N/Fe/N/Fe-Fe/N/Fe/N. (d) Type4: N/Fe/N/Fe-N/Fe/N/Fe.

optimized by using finite element analysis (FEA) under the same machine size and copper loss (20W). Their parameters are listed in TABLE I. Note that for Type1 and Type2, the stator slot number N_s=12 while it is 6 for Type3 and Type4. Fig. 2 compares their air-gap flux density resulted from both PM MMF and armature MMF. As can be seen, both PM field and armature field of four CPM topologies are totally different.

In terms of PM field, the harmonic pole-pair numbers are

$$p_{m,k} = |mp + kN_r| \quad (1)$$

where p is the fundamental pole-pair number of PM MMF, N_r is the rotor pole number, m and k are the orders of Fourier series of PM MMF and permeance harmonics.

Obviously, PM field is largely related to CPM topology since it directly influences p and the order and magnitude of $p_{m,k}$. As listed in TABLE II, for Type1 and Type3, p=N_s/2 due to the different PM locations of the adjacent stator teeth; for Type3 and Type4, p=N_s since the PM locations of all the stator teeth are identical. Correspondingly, the orders and magnitudes of major harmonics (with magnitude larger than 0.2T) of the topologies are all different, Fig. 2.

Considering the winding configurations of different CPM topologies, the equivalent pole-pair number p_{eq} is utilized, thus the windings can be arranged based on the conventional theory of star of slots [8]. Based on TABLE II, p_{eq}=4 for Type1; p_{eq} =2 for Type2; p_{eq}=1 for Type3 and p_{eq}=2 for Type4. When the concentrated windings (CWs) are adopted, the armature fields of four topologies are also compared in Fig. 2. As can be seen, abundant harmonics exist due to the utilization of CWs, rotor-teeth modulation and stator iron-poles modulation. Again, the orders and magnitudes of major harmonics are all different and Type3 and Type4 have higher magnitudes than the other two types, which may produce higher torque.

B. *Torque Contribution of Working Harmonics*

From Fig. 2, it is clear that different CPM topologies have different harmonic pairs of PM field and armature field. To further identify and compare the working harmonic pairs, the torque contribution of each field harmonic is obtained by using Maxwell tensor, as

$$T_n(t) = \pi R_g^2 l B_{rn} B_{tn} \cos[\theta_{rn}(t) - \theta_{tn}(t)] / \mu_0 \quad (2)$$

where $T_n(t)$ is the instantaneous torque produced by the n^{th} harmonic, R_g is the air-gap radius, μ_0 is the vacuum permeability, B_{rn} and $\theta_{rn}(t)$ are the magnitude and phase of the radial component of the n^{th} harmonic, B_{tn} and $\theta_{tn}(t)$ are those of the tangential component.

As can be seen in Fig. 3, the torques of different FRPM machines are all contributed by several field harmonics. However, the orders and their contributions are totally different. For Type1 and Type4, the torque contributions are scattered while those are relatively concentrated for Type2 and Type 3, as highlighted in TABLE III, IV. In addition, Type3 and Type4 are more likely to have higher torque than Type1 and Type2, thanks to the improved armature field. Compared with Type3, the torque of Type4 is higher since more

TABLE I
PARAMETERS OF FRPM MACHINES (UNITS: MM)

	FEA models								Prototypes			
	Type1		Type2		Type3		Type4		Type2		Type4	
	CPM	SPM	CPM	SPM	CPM	SPM	CPM	SPM	CPM	SPM	CPM	SPM
N_s	12				6				12		6	
R_o	45											
l	25											
g	0.5											
h_m	2											
B_r,u_r	1.2T, 1.05											
t_{sy}	2.2	2.1	3.1	3.2	5.8	4.8	4.0	3.3	3.2		4.2	
w_{st}	4.6	4.0	3.5	3.0	7.6	6.8	8.4	7.4	3.2		8.4	
w_{so}	3.2	2.5	2.3	1.9	4.7	4.6	5.0	4.1	2.5			
α_m	0.56	/	0.64	/	0.60	/	0.66	/	0.60	/	0.60	/
R_{ro}	28.1	29.0	27.2	27.7	28.1	26.8	27.2	27.2	26.8			
α_r	0.32	0.27	0.28	0.26	0.27	0.3	0.31	0.28	0.30			

R_o is the stator outer radius, l is the stack length, g is the air-gap length, h_m is the PM thickness, B_r and μ_r are the remanence and relative permeability of the PM material, t_{sy} is the thickness of stator yoke, w_{st} is the width of stator tooth, w_{so} is the width of stator slot opening, α_m is the PM width ratio, R_{ro} is the rotor outer radius, and α_r is the width ratio of rotor tooth.

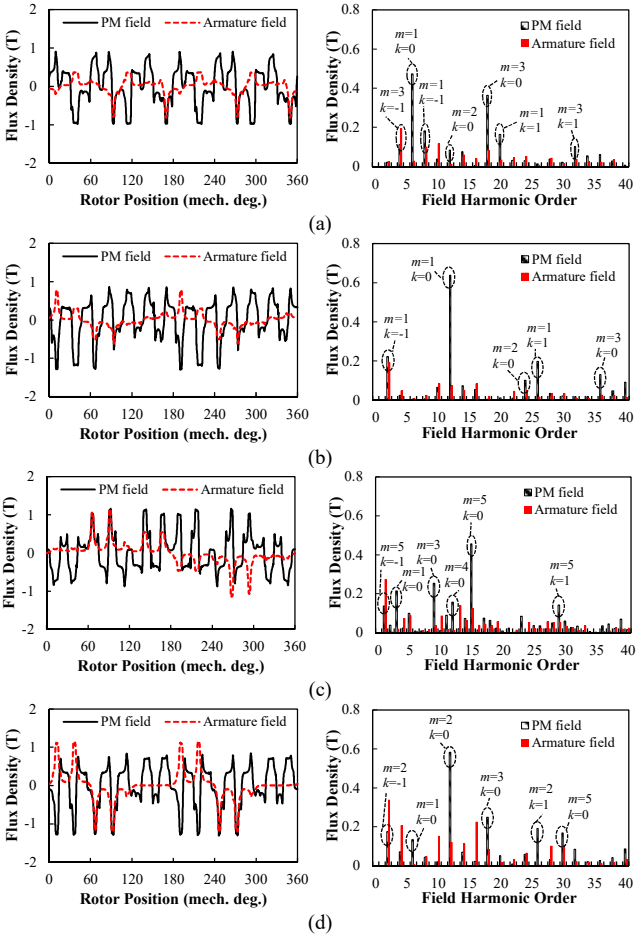

Fig. 2. Field distributions of different CPM topologies (left: waveform, right: harmonic spectrum). (a) Type1. (b) Type2. (c) Type3. (d) Type4.

TABLE II
POLE-PAIR NUMBER OF FRPM MACHINES WITH DIFFERENT CPM TYPES

CPM type	Type1	Type2	Type3	Type4
p	N_s/2	N_s	N_s/2	N_s
Major field harmonics	N_s/2, 3N_s/2	N_s	3N_s/2, 5N_s/2	2N_s, 3N_s
p_{eq}	$\min(\lvert N_s/2 - N_r\rvert, \lvert 3N_s/2 - N_r\rvert)$	$\lvert N_s - N_r\rvert$	$\min(\lvert 3N_s/2 - N_r\rvert, \lvert 5N_s/2 - N_r\rvert)$	$\min(\lvert 2N_s - N_r\rvert, \lvert 3N_s - N_r\rvert)$

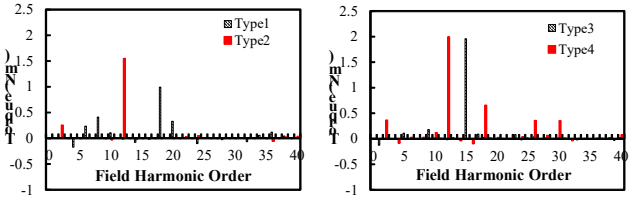

Fig. 3. Torque contribution of field harmonics. (a) Type1, 2. (b)Type3, 4.

TABLE III
TORQUE PROPORTION OF FIELD HARMONICS IN TYPE1 AND TYPE2

	p	p-N_r	p+N_r	$2p$	$2p$-N_r	$2p$+N_r	$3p$	$3p$-N_r	$3p$+N_r
Type1	6th (12%)	8th (22%)	20th (18%)	12th 1%)	(- 2nd (0%)	26th (1%)-	18th (53%)	4th (-9%)	32nd (-4%)
Type2	12th (82%)	2nd (13%)	26th (0%)	24th (3%)	10th (-2%)	38th (1%)	36th (-3%)	22nd (0%)	50th (1%)

TABLE IV
TORQUE PROPORTION OF FIELD HARMONICS IN TYPE3 AND TYPE4

	p	p-N_r	p+N_r	$2p$	$2p$-N_r	$2p$+N_r	$3p$
Type3	3rd (0%)	11th (1%)	17th (4%)	6th (0%)	8th (0%)-	22nd (0%)	9th (8%)
Type4	6th (1%)	8th (1%)	20th (1%)	12th (58%)	2nd (11%)	26th (10%)	18th (19%)
	$3p$-N_r	$3p$+N_r	$4p$-N_r	$5p$	$5p$-N_r	$5p$+N_r	$6p$
Type3	5th (5%)	23rd (4%)	2nd (0%)	15th (89%)	1st (-6%)	29th (0%)	18th (1%)
Type4	4th (-2%)	32nd (-1%)	10th (3%)	30th (10%)	16th (-3%)	44th (-3%)	36th (0%)

harmonic pairs with considerable magnitudes (e.g. the 2nd, 18th, 26th etc.) are utilized.

III. INFLUENCE OF CRITICAL PARAMETERS ON PERFORMANCE

A. *Influence of PM dimensions*

As labeled in Fig. 1, both PM width ratio (a_m=w_m/τ_m) and thickness (h_m) are critical parameters for CPM machines since they directly affect the magnitudes of PM MMF and equivalent air-gap length [14-16]. Based on the parameters in TABLE I, the influence of a_m on average torque of the machines is shown in Fig. 4(a). As can be seen, for each machine, its average torque can be improved by properly increasing a_m from 0.5, but there exists an optimal a_m (normally around 0.6-0.65) due to the saturation of the stator iron poles. In addition, Type4 always has the highest torque while Type1 has the lowest. Fig. 4(b) shows the variation of torque per PM volume against a_m. As can be seen, all the machines achieve the maximum PM utilization ratio when a_m=0.5. In addition, Type4 has the highest torque per PM volume thanks to the high average torque. The influence of h_m on machine performance is shown in Fig. 5. As can be seen, for each CPM topology, there exists an optimal h_m, which is similar as the conventional SPM topology since the rotor-teeth modulation effect deteriorates with h_m [17]. In addition, for all the CPM topologies, the torque per PM volume always decreases with h_m. Again, Type4 has the maximum torque and torque per PM volume.

B. *Influence of Rotor Pole Number*

Fig. 6 shows the influence of rotor pole number N_r on machine average torque. It should be noted that all the machines are globally optimized aiming at maximum torque under the same machine diameter and axial length shown in TABLE I. As can be seen, for Type3, the CPM machine has

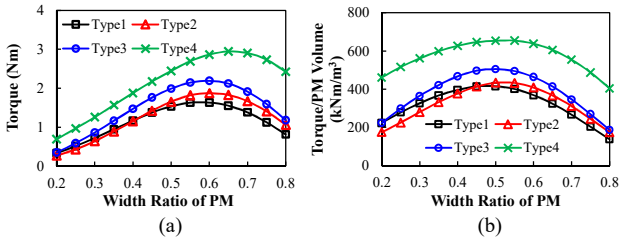

Fig. 4. Influence of a_m on performance. (a) Torque. (b) Torque/PM volume.

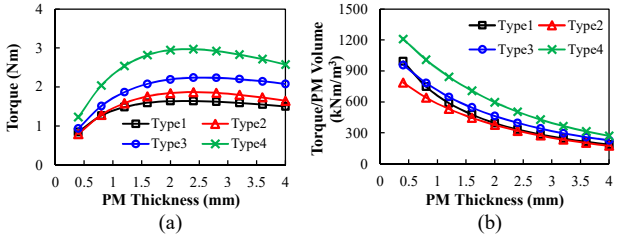

Fig.5. Influence of h_m on performance. (a) Torque. (b) Torque/PM volume.

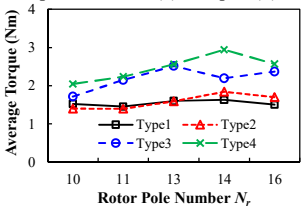

Fig.6. Influence of rotor pole number on average torque.

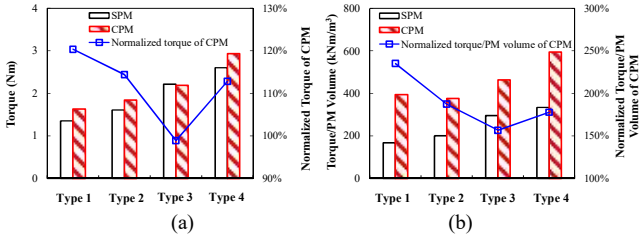

Fig. 7. Performance comparison of FRPM machines with different SPM and CPM topologies. (a) Torque. (b) Torque per PM volume.

maximum torque when N_r=13 while for other three CPM types, the machines have maximum torque when N_r=14.

IV. PERFORMANCE COMPARISON WITH SPM TOPOLOGIES

The SPM counterpart of each CPM topology can be easily obtained by setting a_m =0.5 and replacing the stator iron poles with negatively magnetized PMs [8]. Thus, the torque comparison of FRPM machines with different CPM and SPM topologies is conducted, as shown in Fig. 7. TABLE I lists the optimum parameters of the machines. Although CPM and SPM machines of Type3 have maximum torque with N_r being 13 [8], all the machines in this study are analyzed based on the identical N_r of 14 in order to directly reveal and compare the different working harmonics and saturation conditions of four CPM topologies.

As can be seen from Fig. 7 (a), for either SPM or CPM, 1) the machines with identical PM locations on two adjacent stator teeth are more likely to produce higher torque than those with different PM locations, e.g. for CPM topology, Type2 has 13% higher torque than Type1, Type4 has 34% higher torque than Type3; 2) the machines with two PM pairs on each stator tooth produce higher torque than those with one PM pair, e.g. for CPM topology, Type3 has 34% higher torque than Type1,

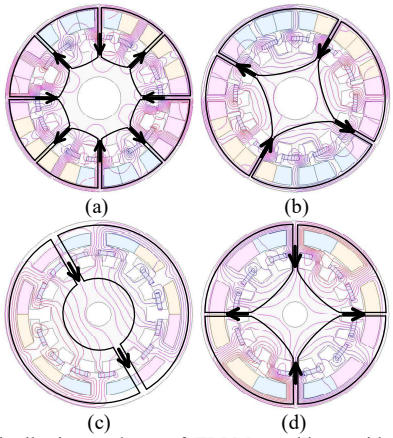

Fig. 8. Flux distribution and p_{eq} of FRPM machines with different CPM topologies. (a) Type1. (b) Type2. (c) Type3. (d) Type4.

Type4 has 60% higher torque than Type2. The conclusions are also applied to the torque per PM volume of the machines, as shown in Fig. 7 (b).

For each machine type, by setting the performance of SPM topology as benchmark, the normalized performance of the CPM topology is shown in Fig. 7. As can be seen, the torque improvement of CPM over SPM is largely related to machine type. In addition to Type3, the torque of all other CPM types can be improved, and Type1 has the largest improvement (by 20%). This phenomenon can be explained by different equivalent pole-pair numbers p_{eq} of the machines, as shown in Fig. 8. For example, p_{eq}=1 for Type3 while it is 2 for Type4. Therefore, the stator yoke of Type3 is more likely to suffer high saturation due to the larger flux per pole caused by the smaller p_{eq}. The improvement of armature field and torque of the CPM topology over SPM topology is then restricted.

By virtue of reduced PM volume as well as improved or similar average torque, the torque per PM volume of all CPM topologies can be largely improved (over 150%), making them suitable for low-cost applications, Fig. 7 (b).

V. Experimental Validation

To validate the analyses, two SPM and two CPM prototypes of Type2 and Type4 are manufactured and tested. Fig.9 shows the machine structures, and TABLE I lists their parameters. For simplicity, all the four prototypes share the same rotor.

Fig. 10 shows the measured and FE-predicted back-EMFs of the machines (n=400rpm). Under the same slot filling factor, the number of series turns per phase n_c is 74 for the Type2-SPM and CPM machines, and it is 115 for the Type4-SPM and CPM machines. For SPM machines, a good agreement between the results can be observed since the measured values of the fundamental back-EMF exceed 93% of the FEA values. For CPM machines, the discrepancies between the results are larger especially for Type4 (the measured value is around 80% of the FE-predicted value). In addition to manufacturing imperfection, this phenomenon can be attributed to the large end-effects in CPM topologies [18, 19], and some techniques should be further considered to reduce the effect. Despite the large end-effects, the improved back-EMFs of CPM topologies can still be verified since both

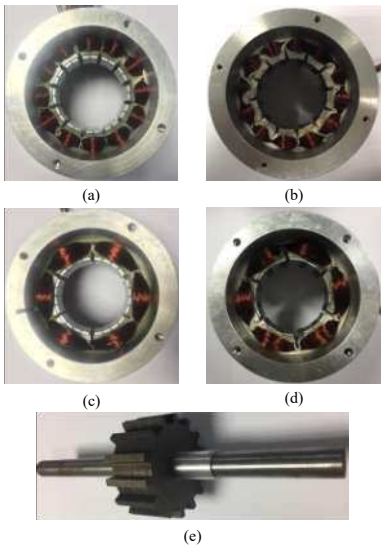

Fig.9. Prototypes. (a) Type2-SPM stator. (b) Type2-CPM stator. (c) Type4-SPM stator. (d) Type4-CPM stator. (e) Shared 14-pole-rotor.

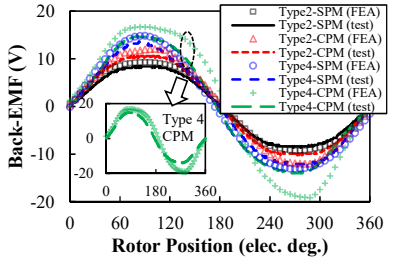

Fig. 10. Measured and FE-predicted back-EMFs. (n=400rpm)

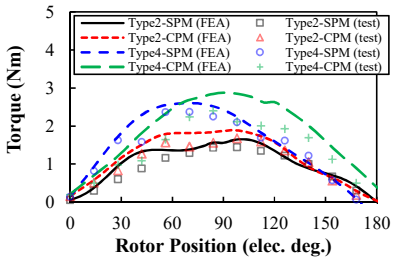

Fig. 11. Measured and FE-predicted static torques. (I_a=-2I_b=-2I_c)

CPM machines have higher measured back-EMFs than their SPM counterparts.

The variation of static torque of the machines can be measured by suppling three-phase windings with fixed dc current (I_a=-2I_b=-2I_c=I_{dc}=I_{rated}, and the rated current I_{rated} is corresponded to p_{cu}=20W) [20], as shown in Fig. 11. Again, for SPM machines, the test results match well with the FEA results while they are obviously lower for CPM machines. However, the measured maximum static torques of the CPM machines are still larger than the SPM machines, albeit with almost halved PM volume, from which the previous analyses can be verified.

VI. Conclusion

In this paper, various FRPM machines with different CPM topologies have been analyzed and compared. It has been found that the working harmonics of CPM machine is largely related to the CPM topology, and the Type4 CPM machine has been proven to exhibit the highest torque. The advantages of

different CPM topologies over their SPM counterparts have also been analyzed and compared. Both FEA and tests have been conducted to verify the findings.

REFERENCES

[1] R. Deodhar, S. Andersson, I. Boldea, and T. J. E. Miller, "The flux reversal machine: A new brushless doubly-salient permanent magnet machine," *IEEE Trans. Ind. Appl.*, vol. 33, no. 4, pp. 925–934, Jul. 1997.

[2] C. Wang, S. A. Nasar, and I. Boldea, "Three-phase flux reversal machine (FRM)," *Proc. Inst. Elect. Eng.—Electr. Power Appl.*, vol. 146, no. 2, pp. 139–146, Mar. 1999.

[3] I. Boldea, J. Zhang, and S. A. Nasar, "Theoretical characterization of flux reversal machine in low speed servo drives-the pole-PM configuration," *IEEE Trans. Ind. Appl.*, vol. 38, no. 6, pp. 1549–1557, Dec. 2002.

[4] Z. Q. Zhu, Z. Z. Wu, D. Evans, and W. Q. Chu, "Novel electrical machines having separate PM excitation stator," *IEEE Trans. Magn.*, vol. 51, no. 4, Apr. 2015.

[5] T. H. Kim, "A study on the design of an inset-permanent-magnet-type flux-reversal machine," *IEEE Trans. Magn.*, vol. 45, no. 6, pp. 2859–2862, May 2009.

[6] T. H. Kim, S. H. Won, K. Bong, and J. Lee, "Reduction of cogging torque in flux-reversal machine by rotor teeth pairing," *IEEE Trans. Magn.*, vol. 41, no. 10, pp. 3964–3966, Oct. 2005.

[7] Y. Gao, R. Qu, D. Li, J. Li, and L. Wu, "Design of three-phase flux-reversal machines with fractional-slot windings," *IEEE Trans. Ind. Appl.*, vol. 52, no. 4, pp. 2856–2864, July 2016.

[8] H. Li and Z. Q. Zhu, "Influence of magnet arrangement on performance of flux reversal permanent magnet machine," in *Int. Conf. Electr. Mach. Drives (IEMDC 2017)*, May 2017.

[9] Y. Gao, R. Qu, D. Li, J. Li, and G. Zhou. "Consequent-pole flux-reversal permanent-magnet machine for electric vehicle propulsion," *IEEE Trans. Appl. Supercond.*, vol. 26, no. 4, June 2016.

[10] K. Atallah, and D. Howe, "A novel high-performance magnetic gear," *IEEE Trans. Magn.*, vol.37, no.4, pp.2844-2846, 2001.

[11] D. S. More and B. G. Fernandes, "Analysis of flux-reversal machine based on fictitious electrical gear," *IEEE Trans. Energy Convers.*, vol. 25, no. 4, pp. 940–947, Dec. 2010.

[12] Z. Z. Wu and Z. Q. Zhu, "Analysis of air-gap field modulation and magnetic gearing effects in switched flux permanent magnet machines," *IEEE Trans. Magn.*, vol. 51, no. 5, p. 8105012, 2015.

[13] M. Cheng, P. Han, and W. Hua, "A general airgap field modulation theory for electrical machines," *IEEE Trans. Ind. Electron.*, vol. 64, no. 8, pp. 6063–6074, 2017.

[14] S. Chung, J. Kim, B. Woo, D. Hong, J. Lee, and D. Koo, "A novel design of modular three - phase permanent magnet vernier machine with consequent pole rotor," *IEEE Trans. Magn.*, vol. 47, no. 10, pp. 4215 - 4218, Oct. 2011

[15] S. Chung, J. Kim, D. Koo, B. Woo, D. Hong, and J. Lee, "Fractional slot concentrated winding permanent magnet synchronous machine with consequent pole rotor for low speed direct drive," *IEEE Trans. Magn.*, vol. 48, no. 11, pp. 2965–2968, 2012

[16] D. G. Dorrell, M. Popescu, and D. M. Ionel, "Unbalanced magnetic pull due to asymmetry and low-level static rotor eccentricity in fractional-slot brushless permanent-magnet motors with surface-magnet and consequent-pole rotors," *IEEE Trans. Magn.*, vol. 46, no. 7, pp. 2675-2685, 2010.

[17] Y. Gao, R. Qu, D. Li, and J. Li, "Torque performance analysis of three-phase flux reversal machines," *IEEE Trans. Ind. Appl.*, vol. 53, no. 3, pp. 2110–2119, Mar. 2017.

[18] Z. Z. Wu and Z. Q. Zhu, "Comparative analysis of end effect in partitioned stator flux reversal machines having surface-mounted and consequent pole permanent magnets," *IEEE Trans. Magn.*, vol. 52, no. 7, July 2016.

[19] J. X. Shen, H. Y. Li, H. Hao, and M. J. Jin. "A coaxial magnetic gear with consequent-pole rotors," *IEEE Trans. Energy Conv.*, vol. 32, no. 1, pp. 267–275, 2017.

[20] Z. Q. Zhu, "A simple method for measuring cogging torque in permanent magnet machines," in *Proc. IEEE Power Energy Soc. Gen. Meet.*, 2009, pp. 1–4.